Co-published by
Institute of Fluid-Flow Machinery
Polish Academy of Sciences
Committee on Thermodynamics and Combustion
Polish Academy of Sciences

http://www.imp.gda.pl/archives-of-thermodynamics/

Numerical study on effect of operating pressures on CRKEC-based two-stage ejector

Virendra Kumar[a], Surendra Kumar Yadav[b*], Anil Kumar[c], Nishant Kumar Singh[a], Lalta Prasad[d]

[a]Department of Mechanical Engineering. Harcourt Butler technical University, Kanpur 208002, India
[b]Department of Mechanical Engineering. K R Mangalam University, Gurugram 122001, India
[c]Department of Mechanical Engineeringg. KNIT, Sultanpur 228118, India
[d]Department of Mechanical Engg. NIT, Uttrakhand 246174, India
*Corresponding author email: surendra.yadav@krmangalam.edu.in

Received: 14.04.2023; revised: 17.05.2023; accepted: 06.12.2023

Abstract

The two-stage ejector mixing-diffuser section in this study was computed using the Redlich-Kwong equation of state. The ejector was designed based on the constant rate of kinetic energy change (CRKEC) approach. The water vapor mixing diffuser profile and flow properties were calculated using a one-dimensional gas dynamic model. For the numerical investigation, the estimated geometrical profile based on the input design and operating conditions was utilized. ANSYS-Fluent 14.0 was employed for the numerical study. The analysis was conducted under both on-design and off-design scenarios using the standard k-ε turbulence model. The impact of operating factors on flow behavior and entrainment ratios was investigated at off-design conditions. The findings demonstrated that the operational total pressures of the primary, secondary, and exit flows are a function of the two-stage ejector (TSE) entrainment ratio. With a higher exit pressure and more secondary/entrained flows, the entrainment ratio increases. However, altering the primary flow pressure in ways other than for the design conditions reduces the entrainment ratio.

Keywords: Ejector; Constant rate of kinetic energy change (CRKEC); Two-stage ejector (TSE); Jet-pump; Mixing-diffuser

Vol. 45(2024), No. 1, 155–164; doi: 10.24425/ather.2024.150448

Cite this manuscript as: Kumar, V., Yadav, S. K., Kumar, A., Singh, N. K., & Prasad, L. (2024). Numerical study on effect of operating pressures on CRKEC-based two-stage ejector. *Archives of Thermodynamics*, 45(1), 155–164.

1. Introduction

The ejector is a simple mechanical device and is essential for industries and society because of environmental concerns, as it has no moving parts and working fluid restrictions. It can also operate with low-pressure temperature steams produced by industrial waste or solar energy. Ejectors enable pumping the fluid, vacuum creation, and compression of gases from lower pressure to higher pressure. The ejector systems can be utilized in heating as a heat pump [1], refrigeration systems [2, 3], rocket engines [4–6], hydrogen refueling systems [7, 8], geothermal power plants [9], vacuum generator [10], gas mixing [11], augmentation of thrust and suppression of noise [12]. The system performances are highly dependable on the performance of the ejector, which is generally low. The ejector performance is generally measured based on the ratio of entrainment capability. The entrainment ratio is the ratio of the entrained fluid mass flow rate to the primary or motive fluid mass flow rate. The ejector entrainment ratio is affected by geometrical parameters, operating parameters, and the working fluid used.

Nomenclature

a, b – Redlich-Kwong constants
A – cross-section area, m^2
c, C – velocity, m/s
C_1, C_2 – Sutherland constants
D – diameter, m
f – Fanning friction factor
G – constant
KE – kinetic energy
K – wall roughness, μm
L_n – nozzle section length, m
$\dot{m}_p$ – primary mass flow rate, kg/s
$\dot{m}_{s1}$ – first entrain mass flow rate, kg/s
$\dot{m}_{s2}$ – second entrain mass flow rate, kg/s
M – Mach number
p, P – pressure, Pa
r – radius, m
R – individual gas constant, kJ/K
Re – Renolds Number
T – temperature, K
v, V – specific volume, m^3/s
x, X – axial distance, m
y, Y – cross-section distance, m

Greek symbols

γ – specific heat ratio
μ – dynamic viscosity, Pa·s
ρ – density, kg/m^3
ϕ – rate of kinetic energy change, kg·m/s^3
ω – entrainment ratio

Subscripts and Superscripts

d – diffuser
i, j, k – space component
n – nozzle
m – mixing
o – stagnation condition
p – primary flow
s – secondary flow
x, y – direction

Numerical tools are widely used to optimize the geometrical and operating parameters. The profile of a single-stage ejector is dependent mainly on the design approaches. Constant pressure mixing (CPM) and constant area mixing (CAM) are the traditional ejector design methodologies [13]. Constant rate of momentum change (CRMC) and constant rate of kinetic energy change (CRKEC) are two methods for designing ejectors that are based on physics [14, 15]. The profile of a typical single-stage conventional ejector is shown in Fig. 1. The parameters optimized by researchers are the area ratio [16], multi ejector refrigerating system [17], convergence angle of the suction chamber [18], diameter of the nozzle throat and mixing section [19]. The entrainment ratio and critical back pressure of the ejectors are influenced by the position of the nozzle exit. According to the CAM and CPM-based ejectors study [20], increased boiler temperature ratios result in increased critical back pressure. By raising the evaporator temperature, the entrainment ratio and critical back pressure rise. The operating parameters optimized by researchers are primary flow total pressures and temperatures [21], secondary flow pressures and temperatures [22], and exit flow total pressures [20].

Recent studies focus on developing physics-based design approaches such as CRMC and CRKEC to improve performance by mitigating loss due to thermodynamic shocks in conventional (CAM and CPM) single-stage ejectors [13]. To further boost the performance, a two-stage ejector is a useful substitution [23–25]. The second entrained stream is driven into the second stage of the ejector using the excess momentum of the discharged flow at the mixing section exit [26]. The physics-based CRMC single-stage ejector performance is further improved by modifying single-stage to two-stage ejectors [27] and others [28–29]. The typical two-stage ejector is shown in Fig. 2.

The literature review shows a gap in using the physics-based CRKEC approach for real fluids in designing a two-stage ejector. This work addresses this gap by modifying the physics-based 1D gas dynamic CRKEC model [15] for single-stage ejector design with the Redlich-Kwong equation of state, to create a model for two-stage ejectors. This modified model, called the 1D gas dynamic TSE model, is used to calculate profiles and flow properties in the mixing-diffuser section. The TSE is further analyzed using ANSYS-Fluent 14.0 at design and operating conditions.

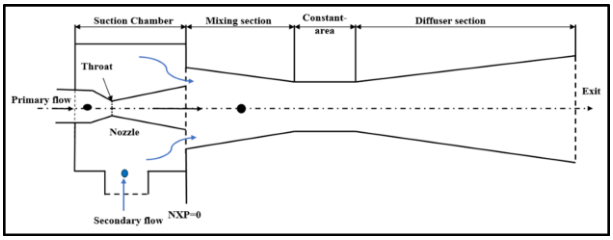

Fig. 1. A schematic diagram of the conventional ejector [27].

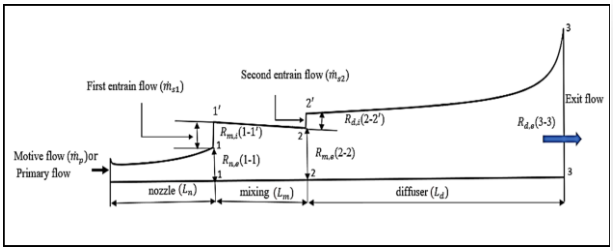

Fig. 2. Two-stage ejector.

2. 1D gas dynamic mixing-diffuser design

The 1D gas dynamic CRKEC design approach [15] was considered a reference to further model the mixing-diffuser two-stage ejector for water vapour. The geometry was considered axisymmetric. The 1D gas dynamic compressible flow mixing-diffuser design model was derived considering the steady-state flow and adiabatic conditions using mass, momentum, and energy equations. The following section lists the equations and their differential forms used to calculate the incremental change in area, pressure, and temperature.

The Mach number and its differential form are given by

$$M^2 = \frac{C^2}{\gamma RT},\ \frac{dM}{M} - \frac{dC}{C} + \frac{dT}{2T} = 0. \tag{1}$$

The equation of state (Redlich Kwong) and its differential form are given by

$$P = \frac{RT}{\frac{V}{n}-b} - \frac{a}{\sqrt{T}\frac{V}{n}\left(\frac{V}{n}+b\right)},\quad dP = [(X)dT + (Y)d\rho], \tag{2}$$

where

$$X = \left[\frac{\rho\,.\,R}{(G-\rho b)} + \frac{1}{2}\left\{\frac{\rho^2.\,a}{T^{1.5}.\,G(G+\rho\,.\,b)}\right\}\right], \tag{2a}$$

$$Y = \left[\frac{RT(G-\rho b)+b\rho RT}{(G-\rho b)^2} - \frac{a}{\sqrt{T}}\left\{\frac{2\rho(G+\rho b)-\rho^2 b}{G(G+\rho b)^2}\right\}\right], \tag{2b}$$

where the Redlich Kwong constants are

$$a = \frac{0.4275R^2T_C^{2.5}}{P_C}, b = \frac{0.0866RT_C}{P_C}. \tag{2c}$$

The conservation of mass has the form:

$$\dot{m} = \rho AC,\quad \frac{d\rho}{\rho} + \frac{dA}{A} + \frac{dC}{C} = 0. \tag{3}$$

The conservation of energy and its differential form for passive adiabatic conditions are as follows

$$T_0 = T + \frac{C^2}{2C_P},\quad dT + \frac{CdC}{C_P} = 0. \tag{4}$$

The conservation of momentum including friction writes as

$$\frac{dP}{P} + \frac{\gamma}{2}M^2\frac{4fdx}{D} + \gamma M^2\frac{dC}{C} = 0, \tag{5}$$

where the local Fanning friction factor f is defined as [15]:

$$f = \frac{0.0625}{\left[log_{10}\left(\frac{K}{3.7D}+\frac{5.74}{R_e^{0.9}}\right)\right]^2}, \tag{5a}$$

where the local Reynolds number is $\mathrm{Re} = \frac{\rho CD}{\mu}$, and $\mu = \frac{C_1T^{1.5}}{T+C_2}$, according to Sutherland's law of viscosity, where C_1 and C_2 are Sutherland's constants.

The following assumptions were made to develop a 1D gas dynamic mathematical model to compute the profile of two-stage ejector mixing-diffuser design and flow properties.

- The working fluid is water vapour. In addition, due to the low operating pressure, the kinetic energy of gas molecules becomes more significant than intermolecular forces and molecular size. Consequently, water vapour can be approximated as an ideal gas in this particular behaviour [30];
- The expected entrainment ratio (ω) is considered;
- At the ejector inlet, the combined pressure and temperature of the primary and secondary flows are known;
- The secondary flow velocity is known;
- Locally, the Fanning friction factor is used to specify the influence of friction.

The baseline equation for CRKEC two-stage ejector mixing-diffuser section design is given by Eq. (6)

$$\frac{d(\dot{K}E)}{dx} = \dot{m}_p(1+\omega)\cdot C_{i,x}\frac{dC}{dx} = \phi, \tag{6}$$

where ϕ is the rate of kinetic energy change, which is considered constant.

The velocity gradient can be calculated using Eq. (7), which is derived from Eq. (1), for a chosen value of ϕ and dx

$$\frac{dC}{C_{i,x}} = \frac{\phi\,dx}{\dot{m}_p(1+\omega){C_{i,x}}^2}. \tag{7}$$

The change in local cross-sectional area of the diffuser at the i^{th} location is given by

$$\frac{dA}{A_{i,x}} = \frac{\gamma}{2}M_{i,x}^2\frac{P_{i,x}}{\rho_{i,x}Y}\frac{4f_{i,x}dx}{D_{i,x}} + \\ + \frac{1}{\rho_{i,x}Y}\left(\gamma M_{i,x}^2\rho_{i,x} - XM_{i,x}^2(\gamma-1)T_{i,x} - \rho_{i,x}Y\right)\frac{\phi\,dx}{\dot{m}_p(1+\omega)C_{i,x}^2}. \tag{8}$$

The change in local pressure of the diffuser at the i^{th} location is given by

$$\frac{dP}{P_{i,x}} = -\rho_{i,x}Y\frac{dA}{A_{i,x}} + \left[XM_{i,x}^2(1-\gamma)T_{i,x} - \rho_{i,x}Y\right]\frac{\phi\,dx}{\dot{m}_p(1+\omega)C_{i,x}^2}. \tag{9}$$

The mixing section produces the most entropy when compared to the nozzle and diffuser of the ejector because it experiences extensive interactions between supersonic primary/motive flow and subsonic (incompressible) entrain/secondary flows. Compounding the mixing section profile is considered crucial compared to other components of ejector design. Further, to model this section, it was considered that mixing takes place at a constant rate, and during mixing, the pressure remains constant (dp=0) [14].

The following equation (10) provides the change in the mixing-diffuser local cross-sectional area at the i^{th} place

$$\frac{dA}{A_{i,x}} = -\frac{1}{\rho Y}\left[XM_{i,x}^2(\gamma-1) + \rho Y\right]\frac{\phi\,dx}{\dot{m}_p(1+\omega){C_{i,x}}^2}. \tag{10}$$

The change in local pressure of the mixing section at the i^{th} location is given by

$$dp = 0. \tag{11}$$

The change in local temperature of the mixing-diffuser at the i^{th} location is given by

$$\frac{dT}{T_{i,x}} = \left[(1-\gamma)M_{i,x}^2\right]\frac{\phi\,dx}{\dot{m}_p(1+\omega){C_{i,x}}^2}. \tag{12}$$

The change in local Mach number of the mixing-diffuser at the i^{th} location can be found from

$$\frac{dM}{M_{i,x}} = \left[1 + \frac{\gamma-1}{2} M_{i,x}^2\right] \frac{\phi\, dx}{\dot{m}_p(1+\omega){c_{i,x}}^2}. \quad (13)$$

Equations (14) and (15) can be used to calculate the total pressure and temperature at the i^{th} position of the mixing-diffuser section, respectively

$$P_{o,i,x} = P_{i,x}\left[1 + \frac{(\gamma-1)}{2} M_{i,x}^2\right]^{\gamma/\gamma-1}, \quad (14)$$

$$T_{o,i,x} = T_{i,x}\left[1 + \frac{(\gamma-1)}{2} M_{i,x}^2\right]. \quad (15)$$

By adding up variations in parameters (*dA*, *dP*, *dM and dT*) for *dx* with parameter's (*A*, *P*, *M*, and *T*) value of its i^{th} location provides the parameter's value at its i+1 location in the flow domain.

3. Computation of geometrical profile and flow parameters

On the basis of Euler's technique, a separate MATLAB programmed was created for each section of the TSE system. The program was used to calculate the geometric coordinates and the attributes of the flow. The input design data which were utilized are shown in Table 1. At each small step (dx=0.5 mm), the variation in radius and the fluid flow characteristics were locally calculated. At the end of the mixing section (2–2) [see Fig. 2] and at the diffuser inlet section (2–2'), equilibrium properties of the incoming primary/motive flow and entrained/secondary flows were first calculated. Appendix A [17] shows the calculations for the equilibrium properties in sections (2–2) and (2–2'). The mixing section was computed by moving from the exit section (2–2) to the inlet section (1–1'), while the diffuser section was calculated by moving from the inlet section (2–2') to the exit section (3–3). The computational process is shown in the flow chart in Fig. 3.

Table 1. Input design and operating parameters of the two-stage ejector.

Parameter	Unit	Value
Motive/primary flow inlet total pressure $P_{o,p}$	Pa	1.91×10^5
Motive/primary flow inlet total temperature $T_{o,p}$	K	396
Motive/primary flow mass flow rate $(\dot{m}_p)$	kg/s	0.001
Entrain/secondary flow inlet total pressure $P_{o,s}$	Pa	872
Entrain/secondary flow inlet total temperature $T_{o,s}$	K	278
Entrain/secondary flow inlet velocity V_s	m/s	50
Individual gas constant (R)	J/kg.K	462
Entrainment ratio(ω)	-	0.42
Wall roughness (K)	m	1.5×10^{-6}
Specific heat ratio (γ)	-	1.3
Working fluid: water vapour		

The value of the CRKEC constant (ϕ) was selected for each section based on no flow separation and no null parameter at its inlet/exit section. The positive value of ϕ was selected because flow accelerates for the nozzle and mixing section while computing from throat to exit of the nozzle and from exit to inlet of mixing. The negative value of ϕ was selected for the diffuser section as the flow decelerated from the inlet to the exit. For the specified design conditions listed in Table 1, the nozzle section was also estimated using the CRKEC technique. Table 2 displays the computed dimensional parameters for the chosen sections of the nozzle, mixing, and diffuser at critical places. Figure 4 and 5 demonstrate, respectively, the variation in the cross- sectional radius of the computed profile of the mixing and diffuser section, and flow characteristics along the mixing diffuser.

4. CFD analysis

The commercial CFD software ANSYS-Fluent is a powerful tool for simulating the problem. The control volume-based technique was used to discretize and solve the governing equations. Numerical equations were solved in space using the second-order upwind approach. The coupled solver with the implicit scheme was used and pressure was linked directly to density to obtain the real physical relations for compressible flow and to capture shock waves.

The computational domain of the TSE system for the CFD simulation was prepared using ANSYS-Workbench. The coordinates of the cross-sectional profile of mixing-diffuser sections were utilized to develop the ejector profile. The computational domain was meshed with a structured quadrilateral. For this kind of mesh, the cell aspect ratio and alignment with the flow domain are easy to control. A relatively higher number of cells were used in the region with higher entropy generation. Fig. 6 displays the created computational domain and its mesh. At the ejector entry and exit, the pressure boundary condition was used, as shown in Table 3. The grid dependency test was run using the standard k-ε turbulence model to determine the best grid size. For testing the ideal grid size under on-design circumstances, the global performance parameter "entrainment ratio" was taken into account. After employing the various mesh sizes (30 000–80 000), it was found that approx. 45 000 cells are suitable for the sake of computational time, accuracy, and cost. The employment of gradient mesh near and inside the mixing region helped predict the boundary layer near the wall and the mixing phenomenon inside the mixing section.

5. Results and discussion

The ANSYS-Fluent simulation results of the computed geometrical profile of TSE are discussed in this section. The complete CFD simulation was performed at zero nozzle exit position (on-design). This section talks about how operating parameters affect flow characteristics and entrainment ratio. The on-design ejector system impacts were predicted by changing one operating parameter at a time.

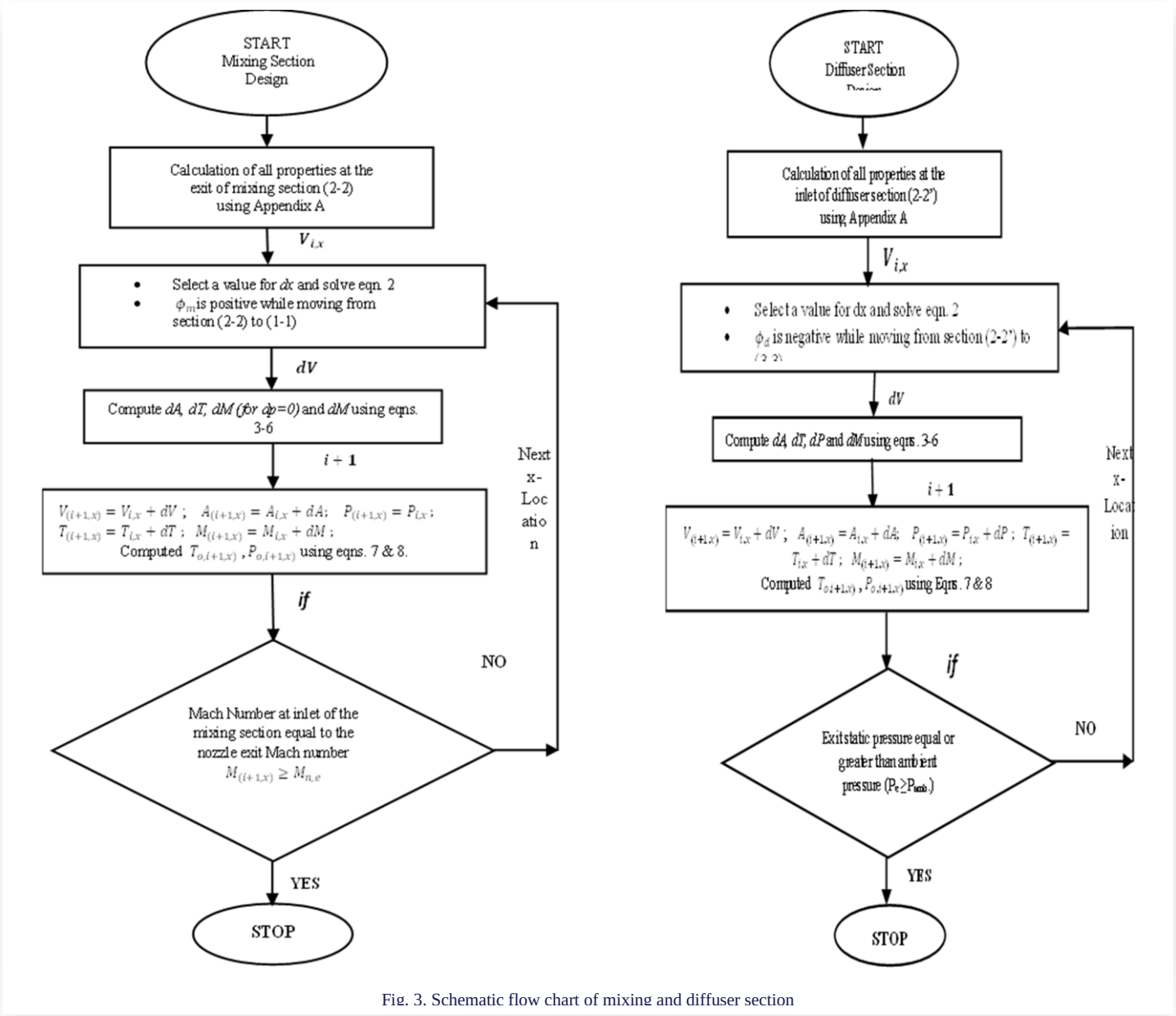

Fig. 3. Schematic flow chart of mixing and diffuser section

Table 2. The dimensional specifications of different sections

Sections	Dimension (mm)
Nozzle	
Inlet radius	2.28
Throat radius	1.01
Exit radius	5.30
Length	100.00
Mixing section	
Inlet radius	11.54
Exit radius	10.06
Length	90.00
Diffuser section	
Inlet radius	13.64
Exit radius	34.66
Length	250

5.1. Effect of exit pressure

The effect of exit pressure has been studied and predicted variations in flow properties and over the entrainment ratio are shown in Figures 7, 8, and 9, respectively. The total pressure at the nozzle intake and the entrained flow (primary and secondary) total pressure at the inlets of the first and second stages were held constant to analyse the impact of exit pressure. Figure 7 depicts the change in centreline static pressure along the mixing-diffuser segment.

The exit pressure directly affects the amount of entrained flow. The pressure and Mach number intense oscillations due to supersonic and subsonic flow mixing inside the mixing chamber are visible but the effect of exit pressure variation on oscillations inside the mixing region is insignificant. However, increasing the exit pressure reduces the Mach number at the exit of the diffuser and helps in pressure recovery at the exit of the diffuser.

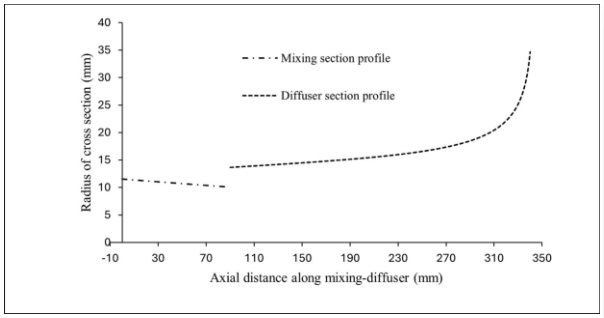

Fig. 4. Variation of cross-section radius along mixing-diffuser section [$\phi_m = -2600\ \mathrm{kgm/s^3}$ and $\phi_d = -550\ \mathrm{kgm/s^3}$].

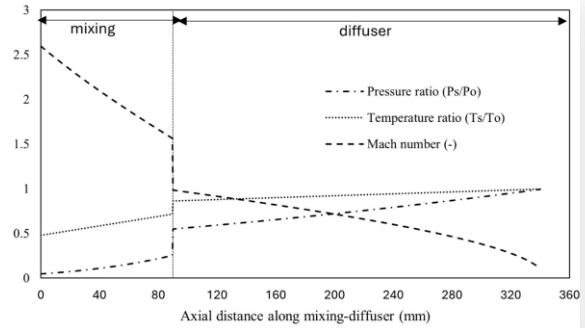

Fig. 5. Variation of flow properties along the mixing-diffuser section [$\phi_m = -2600\ \mathrm{kgm/s^3}$ and $\phi_d = -550\ \mathrm{kgm/s^3}$]

As seen in Figure 9, as the total exit pressure rises and the entrainment ratio falls, the pressure difference between the suction and entrain flow also reduces, which lowers the mass of the entrained flow.

5.2. Effect of entrained flow total pressure

The exit pressure and primary flow total pressure were held constant at on-design conditions in order to analyse the impact of secondary flow total pressure. Figure 10 depicts the change

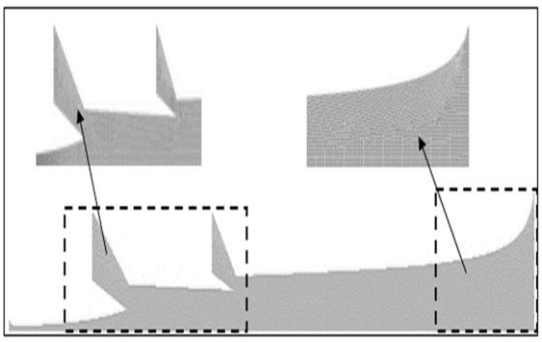

Fig. 6. Computational domain of two-stage ejector

Table 3. Boundary conditions for CFD study.

Section	Boundary Condition	Values
Wall	Adiabatic with no slip	–
Exit	Pressure outlet	$P_{o,e}$=1240 Pa, $T_{o,e}$= 350K
Inlet	Pressure inlet: Primary flow	$P_{o,p}$=191000 Pa, $T_{o,p}$=396K
	Pressure inlet: Secondary flow, stage I and II	$P_{o,s}$=872 Pa, $T_{o,s}$= 278K

in centreline static pressure together with an increase in entrained flow total pressure. With the higher entrained flow total pressure, the amplitude of pressure oscillations in the mixing region is lower compared to lower entrained flow total pressure. The secondary flow total pressure does not allow enough space to expand the primary jet inside the mixing region. In other words, the expansion of the combined jet decreases with an increase in secondary flow total pressure. It is also observed that after the intense interactions of primary and entrain flows, the static pressure gradually increases in the diffuser section.

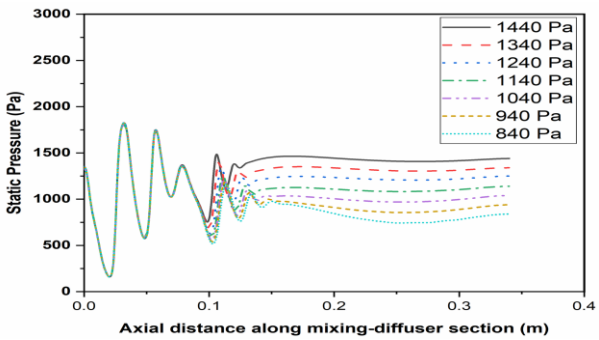

Fig. 7. Variation in static pressure with exit pressure.

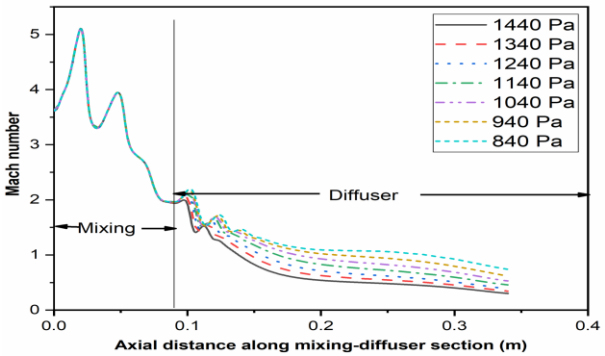

Fig. 8. Variation in Mach number with exit pressure.

With various entrain flow total pressures along the mixing-diffuser, the fluctuation in centreline Mach number is depicted in Figure 11. In the supersonic range, the compression and expansion waves are visible. Additionally, the combined Mach

number grows as the entrain total flow pressure increases. However, the Mach number drops along the mixing-diffuser segment.

Figure 12 illustrates how the two-stage ejector entrainment ratio grows with an increase in entrain flow total pressure. Lower entrainment ratios are produced as a result of the expansion of the primary/motive jet flow expansion wave in the mixing area, which is made possible by the lower entrain total flow pressure.

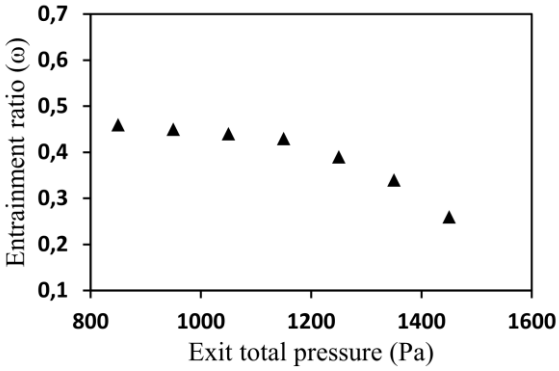

Fig. 9. Variation in entrainment ratio with exit pressures.

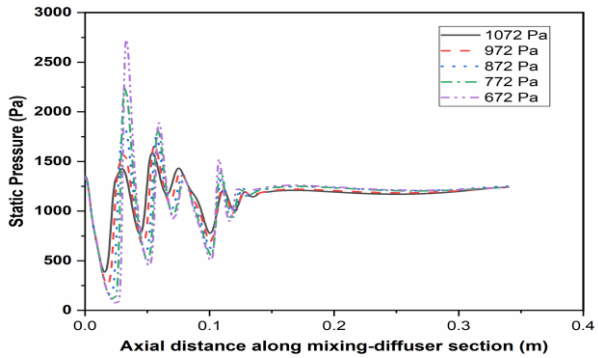

Fig. 10. Variation in static pressure with entrain flow total pressure.

5.3. Effect of primary flow total pressure

Figure 13 depicts the projected centerline static pressure variation along the mixing diffuser for various primary flow total pressures. With an increase in primary flow total pressure, the flow momentum rises. Due to the intensive flow interaction between the high-speed (supersonic) primary flow and the low-speed (subsonic) entrain flows, pressure oscillations are seen inside the mixing region. For larger primary flow total pressures, the pressure oscillation in the mixing region is higher.

The primary flow overall pressure is what causes the momentum to grow. With a sizable expansion angle, it quickens the primary flow at the nozzle exit. Figure 14 demonstrates how the increasing total pressure causes a higher Mach number as the primary flow increases. Figure 15 depicts how the primary flow total pressure affects the entrainment ratio. When the entrainment ratio varies with decreasing primary flow total pressure values, the system is operating at sub-critical conditions because

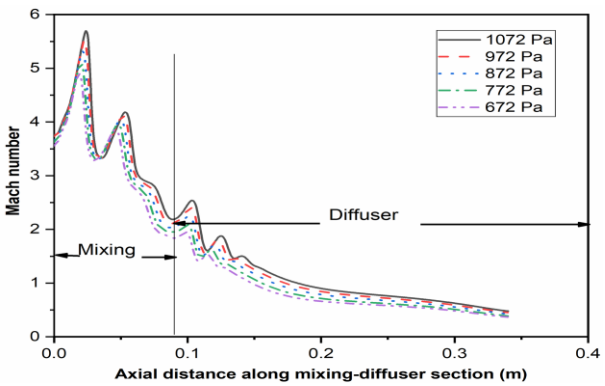

Fig. 11. Variation in Mach number with entrain flow total pressure.

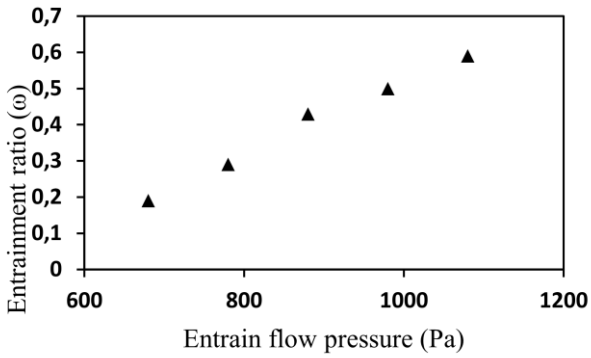

Fig. 12. Variation in entrainment ratio with entrain total flow pressure.

the ejector system operates with a low-pressure differential (below on-design). Entrain flows are proportionately and extremely sensitive to primary flow total pressures in this scenario. When the system enters its critical mode of operation, which in this case is on-design, the optimum entrainment ratio occurs. The pressure difference between the primary flow and ejector output indicates that the system operates above critical conditions when the primary flow pressure is higher (above on-design). In these circumstances, entrainment is reduced because the secondary flow is less sensitive to the total pressure of the primary flow.

6. Conclusions

To create a two-stage ejector, the 1D gas dynamic CRKEC method for water vapour was developed. Based on the CRKEC technique at design operating conditions, the variations in radius and flow characteristics along the mixing-diffuser section of the two-stage ejector are computed. Utilizing ANSYS-Fluent software, the computed geometrical profile of the ejector is numerically analysed. A two-stage ejector response to operating circumstances has been discussed. Due to compression and expansion in the mixing zone, strong interactions have been seen in the entrainment region. After a period of intensive interaction, equilibrium is reached in the mixing section flow. After achieving equilibrium, the diffuser centerline pressure and Mach number progressively change. The primary, entrained and exit flow

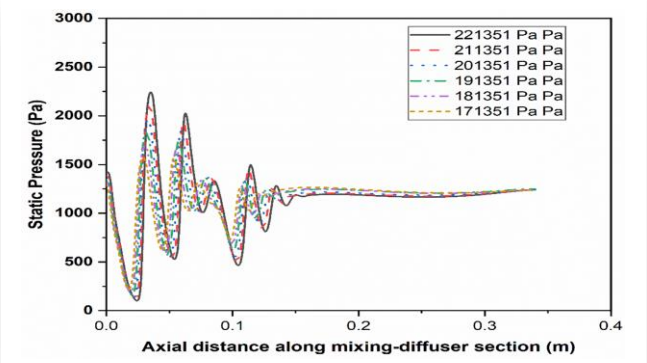

Fig. 13. Variation in static pressure with primary flow total pressure.

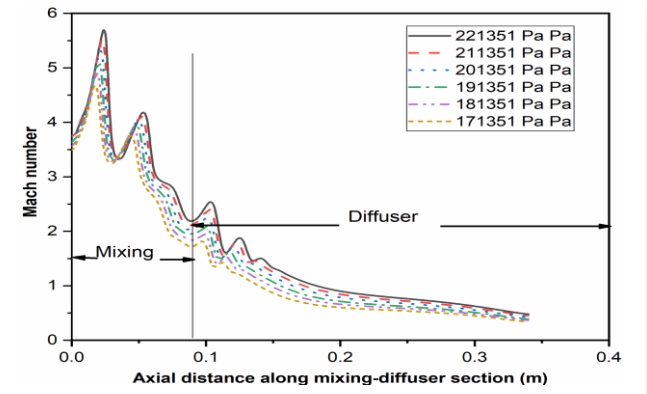

Fig. 14. Variation in Mach number with primary flow total pressure.

pressures of the two-stage ejector are related to the global performance metric "entrainment ratio". It rises when the entrain flow total pressure is raised and falls when the exit flow total pressure is raised. The entrainment ratio of TSE is maximum at on-design (1.91 bar) flow primary flow total pressure. Running the system in other than the on-design primary flow total pressure reduces its performance. However, before the actual field application, a detailed experimental study at on and off-design conditions is needed on the CRKEC-based TSE system. The CRKEC approach has limitations, such as assuming that fluid properties remain constant throughout the system. It may not accurately predict fluid behaviour in systems with complex geometries or strong non-ideal effects, like heat transfer and compression. Thus, further experimental validation is required to support this approach.

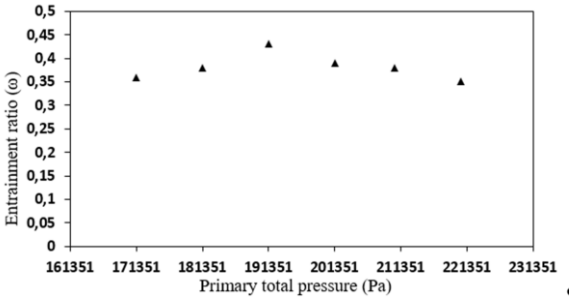

Fig. 15 Variation in entrainment ratio with primary flow total pressure.

Acknowledgements

The authors want to show their gratitude and acknowledge the use of computational facilities in the CFD lab of the Mechanical Engineering Department of Kamla Nehru Institute of Technology, Sultanpur, Uttar Pradesh, India.

Appendix A [15]

Calculation of flow properties at the mixing section exit (2–2).

The essential thermodynamic flow properties at the exit of the mixing section (2–2) as in Fig. 2 were computed based on the following considerations:

- The exit velocity ia an equal-weighted average of the motive/primary and entrain/secondary fluid velocities;
- The combined fluid total temperature at the exit of the adiabatic mixing section is the same as the weighted average of the primary and entrain flows.

The mixed flow velocity is given by

$$C_{2-2} = \frac{C_{n,e}+\omega\, C_S}{1+\omega}. \quad \text{(A.1)}$$

The mixed flow total temperature is given by

$$T_{o,2-2} = \frac{T_{o,p}+\omega T_{o,S}}{1+\omega}. \quad \text{(A.2)}$$

The mixed flow static temperature is given by

$$T_{2-2} = T_{o,2-2} - \frac{c_{2-2}^2}{2c_p}. \quad \text{(A.3)}$$

The mixed fluid total pressure is given by

$$P_{o,2-2} = P_{2-2}\left(\frac{T_{o,2-2}}{T_{2-2}}\right)^{(\gamma/(\gamma-1))}. \quad \text{(A.4)}$$

The mixed flow Mach number is given by

$$M_{2-2} = \frac{C_{2-2}}{\sqrt{\gamma R T_{2-2}}}. \quad \text{(A.5)}$$

The diameter at the exit of the mixing section is given by

$$D_{2-2} = \sqrt[2]{\frac{\dot{m_p}\,(1+\omega)RT_{2-2}}{\pi P_{2-2} C_{2-2}}}. \quad \text{(A.6)}$$

Calculation of flow properties at the inlet of the diffuser (2–2')

The essential flow properties at the inlet of the diffuser section (2–2') as in Fig. 2 were computed by making the following modifications in the formulation for sections (2–2).

$$C_{n,e} \rightarrow C_{m,e},$$

$$\omega_1 \rightarrow \omega_2 = \frac{\dot{m}_{s2}}{\dot{m}_{m,e}},$$

where

$$\dot{m}_{m,e} = \dot{m}_p + \dot{m}_{s2},$$

$$T_{0,p} \rightarrow T_{0,m},$$

$$T_{0,s1} \rightarrow T_{0,s2},$$

$$P_{0,s1} \rightarrow P_{0,s2}$$

and

$$\rho_{0,s1} \rightarrow \rho_{0,s2,}.$$

References

[1] Zhang, B., Wang, Y., Kang, L., & Lv, J. (2013). Study of an innovative ejector heat pump boosted district heating system. *Applied Thermal Engineering*, 58, 98–110. doi: 10.1016/j.applthermaleng.2013.04.021

[2] Jeon, Y., Lee, D., & Cho, H. (2022). Optimisation of motive nozzle position in a modified two-phase ejector expansion household refrigeration cycle using an artificial neural network. *Energy Reports*, 8, 1114–1123. doi: 10.1016/j.egyr.2021.12.033

[3] Cheng, Y., Wang, M., & Yu, J. (2021). Thermodynamic analysis of a novel solar-driven booster-assisted ejector refrigeration cycle. *Solar Energy*, 218, 85–94. doi:10.1016/j.solener.2021.02.031

[4] Yang, Q., Shi, W., Chang, J., & Bao, W. (2015). Maximum thrust for the rocket-ejector mode of the hydrogen fueled rocket-based combined cycle engine. *International Journal of Hydrogen Energy*, 40(9), 3771–3776. doi: 10.1016/j.ijhydene.2015.01.033

[5] Gu, R., Sun, M., Cai, Z., Li, P., & Huang, Y. (2021). Numerical modeling and experimental investigation on the rocket-ejector system with limited mixer length. *Acta Astronautica*, 182, 13–20. doi: 10.1016/j.actaastro.2021.01.055

[6] Gu, R., Sun, M., Cai, Z., Chen, J., Li, P., Dong, Z., Wang, T., Yao, Y., & Huang, Y. (2021). Experimental study on the rocket-ejector system with a throat in the secondary stream. *Aerospace Science and Technology*, 113, 106697. doi: 10.1016/j.ast.2021.106697

[7] Rogie, B., Wen, C., Kaern, M. R., & Rothuizen, E. (2021). Optimisation of the fuelling of hydrogen vehicles using cascade systems and ejectors. *International Journal of Hydrogen Energy*, 46(14), 9567–9579. doi:10.1016/j.ijhydene.2020.12.098

[8] Rogie, B., Kaern, M. R., Wen, C., & Rothuizen, E. (2021). Numerical optimisation of a novel gas-gas ejector for fuelling of hydrogen vehicles. *International Journal of Hydrogen Energy*, 45(41), 21905–21919. doi:10.1016/j.ijhydene.2020.05.169

[9] Mondal, S., Sahana, C., & De, S. (2022). Optimum operation of a novel ejector assisted flash steam cycle for better utilisation of geothermal heat. *Energy Conversion and Management*, 253, 115–164. doi: 10.1016/j.enconman.2021.115164

[10] Xue, H., Wang, L., Jia, L., Xie, C., & Lv, Q. (2020). Design and investigation of a two-stage vacuum ejector for MED-TVC system. *Applied Thermal Engineering*, 167, 114–713. doi: 10.1016/j.applthermaleng.2019.114713

[11] Hailun, Z., Sun, W., Xue, H., Wang, L., & Jia, L. (2021). Performance analysis and prediction of ejector-based hydrogen recycle system under variable proton exchange membrane fuel cell working conditions. *Applied Thermal Engineering*, 197, 117–302. doi: 10.1016/j.applthermaleng.2021.117302

[12] Ye, W., Zhang, J., Xu, W., & Zhang, Z. (2020). Numerical investigation on the flow structures of the multi-strut mixing enhancement ejector. *Applied Thermal Engineering*, 179, 115–653. doi: 10.1016/j.applthermaleng.2020.115653

[13] Keenan, J. H., & Neumann, E. P. (1942). A simple air ejector. *Journal of Applied Mechanics*, 9(2), A75-A8. doi: 10.1115/1.4009187

[14] Kumar, V., Singhal, G., & Subbarao, P. M. V. (2013). Study of supersonic flow in a constant rate of momentum change (CRMC) ejector with frictional effects. *Applied Thermal Engineering*, 60(1-2), 61–71. doi: 10.1016/j.applthermaleng.2013.06.045

[15] Kumar, V., Singhal, G., & Subbarao, P. M. V. (2018). Realisation of novel constant rate of kinetic energy change (CRKEC) supersonic ejector. *Energy*, 164, 694–706. doi: 10.1016/j.energy.2018.08.184

[16] Gu, W., Wang, X., Wang, L., Yin, X., & Liu, H. (2019). Performance investigation of an auto-tuning area ratio ejector for MED-TVC desalination system. *Applied Thermal Engineering*, 155, 470–479. doi: 10.1016/j.applthermaleng.2019.04.018

[17] Aligolzadeh, F., & Hakkaki-Fard, A. (2019). A novel methodology for designing a multi-ejector refrigeration system. *Applied Thermal Engineering*, 151, 26–37. doi: 10.1016/j.applthermaleng.2019.01.112

[18] Ramesh, A. S., & Sekhar, S. J. (2018). Experimental and numerical investigations on the effect of suction chamber angle and nozzle exit position of a steam-jet ejector. *Energy*, 164, 1097–1113. doi: 10.1016/j.energy.2018.09.010

[19] Mohammadi, A. (2019). An investigation of geometrical factors of multi-stage steam ejectors for air suction. *Energy*, 186, 115–808. doi: 10.1016/j.energy.2019.07.138

[20] Aidoun, Z., & Ouzzane, M. (2004). The effect of operating conditions on the performance of a supersonic ejector for refrigeration. *International Journal of Refrigeration*, 27(8), 974–984. doi: 10.1016/j.ijrefrig.2004.05.006

[21] Kuo, J. K., & Hsieh, C. Y. (2021). Numerical investigation into effects of ejector geometry and operating conditions on hydrogen recirculation ratio in 80 kW PEM fuel cell system. *Energy*, 233, 121100. doi: 10.1016/j.energy.2021.121100

[22] Poirier, M. (2022). Influence of Operating Conditions on the Optimal Nozzle Exit Position for Vapor Ejector. *Applied Thermal Engineering*, 210, 118377. doi: 10.1016/j.applthermaleng.2022.118377

[23] Ghorbani, B., Ebrahimi, A., Moradi, M., & Ziabasharhagh, M. (2021). Continuous production of cryogenic energy at low-temperature using two-stage ejector cooling system, Kalina power cycle, cold energy storage unit, and photovoltaic system. *Energy Conversion and Management*, 227, 11354. doi: 10.1016/j.enconman.2020.113541

[24] Wang, P., Ma, H., Spitzenberger, J., Abu-Heiba, A., & Nawaz, K. (2021). Thermal performance of an absorption-assisted two-stage ejector air-to-water heat pump. *Energy Conversion and Management*, 230, 113761. doi: 10.1016/j.enconman.2020.113761

[25] Yan, J., Wen, N., Wang, L., Li, X., Liu, Z., & Li, S. (2018). Optimisation on ejector key geometries of a two-stage ejector-based multi-evaporator refrigeration system. *Energy Conversion and Management*, 175, 142–150. doi: 10.1016/j.enconman.2018.08.110

[26] Kong, F., & Kim, H. D. (2016). Optimisation study of a two-stage ejector–diffuser system. *International Journal of Heat and Mass Transfer*, 101, 1151–1162. doi: 10.1016/j.enconman.2018.08.110

[27] Yadav, S. K., Pandey, K. M., Kumar, V., & Gupta, R. (2021). Computational analysis of a supersonic two-stage ejector. *Materials Today: Proceedings*, 38, 2700–2705. doi: 10.1016/j.matpr.2020.08.483

[28] Domairry, G., & Aziz, A. (2009). Approximate Analysis of MHD squeeze flow between two parallel disks with suction or injection by homotopy perturbation method. *Mathematical Problems in Engineering*. doi: 10.1155/2009/603916

[29] Izadi, M., Yüzbaşı, Ş., & Adel, W. (2021). Two novel Bessel matrix techniques to solve the squeezing flow problem between infinite parallel plates. *Computational Mathematics and Mathematical Physics*, 61(12), 2034–2053. doi: 10.1134/s096554252131002x

[30] Dong, J., Hu, Q., Yu, M., Han, Z., Cui, W., Liang, D., Ma, H., & Pan, X. (Year). Numerical investigation on the influence of mixing chamber length on steam ejector performance. *Applied Thermal Engineering*, 174, 115204. doi.org/10.1016/j.applthermaleng.2020.115204